8. J. T. Trauger, *Bull. Am. Astron. Soc.* **16**, 712 (1984); N. M. Schneider, *ibid.*, p. 663; M. E. Summers *et al.*, *Astrophys. J.* **343**, 468 (1989).
9. N. M. Schneider, thesis, University of Arizona (1988).
10. The instrument uses narrow-band filters to isolate emissions from specific species and to limit the entrance of scattered light from Jupiter. A Lyot mask eliminates diffraction from the secondary mirror support. The CCD (charge-coupled device) detector is a test version for the Hubble Space Telescope Wide-Field Planetary Camera, and uses a Texas Instruments 800 × 800 pixel chip.
11. Detectability is minimized near Jupiter, due to (i) high-scattered light, (ii) unfavorable projection geometry, and (iii) minimal solar flux for scattering, as the radial velocity relative to the sun (and Fraunhofer lines) is small.
12. The supply of fast sodium atoms in Fig. 1 may be estimated from the flux of atoms crossing a vertical plane seen edge-on approximately 7 R_j west of Jupiter. Sodium will be crossing the plane at 60 km s^{-1} at a wide variety of angles; we assume an average angle of 45°, yielding velocities of ~40 km s^{-1} perpendicular and parallel to the plane. At these velocities, sodium is Doppler-shifted out of the solar Fraunhofer line and will scatter the full continuum intensity. The peak D_1 emission rate at this distance (~300 R) therefore implies a column abundance of 1×10^9 Na cm^{-2}. The fast sodium flux is the product of the peak column abundance, the vertical full-width–half-maximum of the emission (~3 R_j), and the velocity perpendicular to the plane, yielding 9×10^{25} Na* s^{-1}. Recombination ejects sodium at all angles around the torus, some of which will never intersect this selected plane; we estimate the total supply to be double the flux observed at this location, for a total ~2×10^{26} Na* s^{-1}. Until the emissions are better modeled, we consider this number uncertain to a factor of several.
13. B. A. Goldberg, G. W. Garneau, S. K. LaVoie, *Science* **226**, 512 (1984) (figure 5, top); C. B. Pilcher *et al.*, *Astrophys. J.* **287**, 427 (1984) (figure 7). The fast sodium features may have been difficult to detect due to rapid changes during the long exposure times previously required.
14. W. D. Cummings, A. J. Dessler, T. W. Hill, *J. Geophys. Res.* **85**, 2108 (1980).
15. Centrifugal forces on the ambient ions will confine them more closely to the equator than the electrons. A small ambipolar electric field will result [J. J. Angerami and J. O. Thomas, *J. Geophys. Res.* **69**, 4537 (1964)] which could slow the motions of the fresh ions.
16. The plasma plane is slightly warped due to nondipolar components of magnetic field, seen by Pioneer and Voyager in the magnetic field measurements [M. H. Acuña, K. W. Behannon, J. E. P. Connerney, in *Physics of the Jovian Magnetosphere*, A. J. Dessler, Ed. (Cambridge Univ. Press, New York, 1983), pp. 1–50], and in recent cold torus observations [J. T. Trauger *et al.*, *Eos* **72**, 184 (1991), and paper in preparation].
17. We assume the recombination rate is comparable to NO^+, tabulated by J. B. A. Mitchell and J. W. McGowan, in *Physics of Ion-Ion and Electron-Ion Collisions*, F. Brouillard and J. W. McGowan, Eds. (Plenum Press, New York, 1983), pp. 279–324. The ionization rate for NaO is calculated using the values for Na [L. J. Kieffer and G. H. Dunn, *Rev. Mod. Phys.* **38**, 1 (1966)] and O [E. Brook *et al.*, *J. Phys. B.* **11**, 3115 (1978)], and the modified sum rule [J. W. Atvos and D. P. Stevenson, *J. Am. Chem. Soc.* **78**, 546 (1956)].
18. R. A. Brown and N. M. Schneider, *Icarus* **48**, 519 (1981).
19. Ions which have equilibrated to the centrifugal equator will corotate in the $\mathbf{\Omega} \times \mathbf{r}$ direction ($\mathbf{\Omega} \equiv$ Jupiter's rotation vector), that is, not strictly perpendicular to **B**. Their thermal motions are non-negligible: charge-exchange products will spray forward into a cone extending about 25° from Io's orbital vector (*22*).
20. The maximum emission attributable to charge exchange (in Fig. 1, for example) is all emission north of the orbital plane between 6.5 to 7.5 R_j west of Jupiter, plus an equivalent amount to the south postulated to underlie the fast sodium released by recombination. The charge exchange supply rate is calculated following the method in (*12*). This upper limit is probably too high, since it assumes no recombination-generated sodium travels north, and that no slow sodium is present in the region.
21. D. M. Hunten, *Geophys. Res. Lett.* **12**, 271 (1985); M. Moreno *et al.*, *Icarus*, in press.
22. M. Mendillo *et al.*, *Nature* **348**, 312 (1990).
23. F. P. Fanale, W. B. Banerdt, L. S. Elson, T. V. Johnson, R. W. Zurek, in *Satellites of Jupiter*, D. Morrison, Ed. (Univ. of Arizona Press, Tucson, 1982), pp. 756–781; D. B. Chrisey, R. E. Johnson, J. W. Boring, J A. Phipps, *Icarus* **75**, 233 (1981).
24. Interested scientists may obtain one copy of a 5-minute VHS videotape containing movies of the data by sending two blank cassettes (the extra to defray duplication expenses) to the first author. The tape is for illustrative purposes only, and is not to be used for scientific analysis.
25. We gratefully acknowledge A. I. F. Stewart, F. Bagenal, M. McGrath, D. Hunten, J. Richardson, and many members of the International Jupiter Watch for discussion and encouragement. We thank Catalina Observatory (University of Arizona) for extensive use of the telescope. This work has been supported by grants from NASA's Planetary Astronomy and Planetary Atmospheres programs. N.M.S. is supported by the National Science Foundation's Presidential Young Investigator Program.

27 June 1991; accepted 7 August 1991

The Temperature of Cavitation

EDWARD B. FLINT AND KENNETH S. SUSLICK*

Ultrasonic irradiation of liquids causes acoustic cavitation: the formation, growth, and implosive collapse of bubbles. Bubble collapse during cavitation generates transient hot spots responsible for high-energy chemistry and emission of light. Determination of the temperatures reached in a cavitating bubble has remained a difficult experimental problem. As a spectroscopic probe of the cavitation event, sonoluminescence provides a solution. Sonoluminescence spectra from silicone oil were reported and analyzed. The observed emission came from excited state C_2 (Swan band transitions, $d^3\Pi_g - a^3\Pi_u$), which has been modeled with synthetic spectra as a function of rotational and vibrational temperatures. From comparison of synthetic to observed spectra, the effective cavitation temperature was found to be 5075 ± 156 K.

HIGH-INTENSITY ULTRASOUND provides a unique interaction between energy and matter. As a consequence, sonochemistry and sonoluminescence have been intensely studied over the past few years (*1–5*). Acoustic cavitation is the primary mechanism of sonoluminescence: the nearly adiabatic compression of gas bubbles during cavitation generates enormous local heating (*1, 2, 6–9*). From the calculations of Lord Rayleigh (*10*) through to those of present-day investigators (*6–9*), peak temperatures of thousands of degrees have been predicted, but there has been only limited experimental confirmation (*1, 4, 11, 12*). We have examined the ro-vibronic sonoluminescence of excited state C_2 as a direct probe of cavitation and have used it to determine the effective temperature of cavitation bubble collapse. Our methodology of temperature measurement has been adapted from flame and plasma techniques based on the rotational and vibrational fine structure of diatomic emission spectra (*13*).

For these studies, we have utilized medium-resolution sonoluminescence spectra from excited state C_2. Emission from the Swan bands of C_2 ($d^3\Pi_g - a^3\Pi_u$) is seen from many organic liquids during ultrasonic irradiation under Ar (*12*). For these studies, sonoluminescence from silicone oil was chosen because of its high intensity. Observed sonoluminescence spectra, calculated synthetic spectra, and the resulting difference spectra for the $\Delta v = +1$ and $\Delta v = 0$ transitions of the Swan bands of C_2 are presented in Figs. 1 and 2, respectively.

The synthetic spectra generated for this work are based on the well-understood theory (*14*) of diatomic-molecule emission. The emission intensity in photons (I) of a single rotational line in a ro-vibronic manifold of a diatomic molecule is given in Eq. 1

$$I \propto \nu^4 AS \exp\{(-hc/k)[(G/T_v) + (F/T_r)]\} \quad (1)$$

where ν is the energy of the transition in cm^{-1}, A is the Franck-Condon factor for the vibrational transition, S is the line strength (*15*), G is the energy of the vibrational state, F is the energy of the rotational state above the vibrational state, T_v is the vibrational temperature, and T_r is the rotational temperature. More common methods of calculating spectroscopic temperatures with this equation could not be used because the low intensity of the sonoluminescence permitted only medium resolution with the spectrometer (*16*). Instead, the spectra presented here were modeled with

School of Chemical Sciences, University of Illinois at Urbana-Champaign, Urbana, IL 61801.

*To whom correspondence should be addressed.

the method of Spier *et al.* (*17*) for overlapping, dense spectral bands. In this procedure, the intensity of each relevant rotational line is calculated, and the contribution of each line on the spectrum is weighted by a triangular aperture function that reflects the resolution of the spectrometer. The wave number and intensity of all the transitions with v'' up to 10 and J'' up to 120 were calculated. Spectra, as they would appear on the 512-element diode array, were calculated from these lines. These calculations have three adjustable parameters for each spectrum: T_v, T_r, and the spectrometer aperture (set to 55 cm^{-1} for the spectra in Figs. 1 and 2). Molecular constants (*14*), Franck-Condon factors (*18*), and Hönl-London formulae (*15*) were taken from the literature.

Synthetic spectra were generated for ranges in T_v of 4500 to 5500 K and in T_r of 4500 to 5500 K. We have presented only the thermally equilibrated case ($T_v = T_r$). Full thermal equilibration of excited-state C_2 molecules is probable before emission because of the long intrinsic lifetime of C_2 [~100 ns (*19*)] and the high pressures of the cavitation event [~1 kbar (*6–9*)], with some caveats (*20, 21*). Separate determinations of vibrational and rotational temperatures are possible in principle; ambiguities in the baseline correction used for the underlying continuum, however, permitted fits between observed spectra and synthetic spectra with rotational temperatures varying from 4600 to 5300 K.

The optimal synthetic spectra were determined by variation of the temperature parameter until the sum of the squares of the residuals was minimized. The temperature of the best fit synthetic spectra are 4900 K for the $\Delta v = +1$ sequence and 5125 K for the $\Delta v = 0$ sequence, as shown in Figs. 1 and 2, respectively. A third, independent determination of the effective temperature, from the ratio of the intensities of the two bands, yielded a temperature estimate of 5200 K. In each case, the statistical error associated with the fitting procedure (as calculated by the Gramm-Schmidt method) was less than ±20 K. The experimental error is more reasonably estimated from the range of the three independent determinations. Thus, the effective temperature of the cavitation events responsible for sonoluminescence under these conditions is T = 5075 ± 156 K (± SD).

Theoretical hydrodynamic models of cavitation have often been used to predict the temperature reached during collapse (*6–9*). Such models, however, are highly variable and sensitive to assumed boundary conditions. Consequently, the temperature predictions have ranged widely, from about 1,000 K to more than 10,000 K. Most prior experimental attempts to measure cavitation temperatures have proved unreliable (*22*); some have attempted to fit unresolved sonoluminescence spectra to blackbody radiation [which it definitively is not (*3, 12*)]; others have examined emission from species produced by secondary chemical processes outside of the cavity (such as alkali metal atom emission in water solutions).

A reliable experimental determination of the temperature of sonochemical reactions (*11*) gave a value of 5200 ± 500 K for the gas phase of the cavitation event in alkane solvents at 5.0 torr vapor pressure under a static pressure of Ar. That determination used a laborious comparative rate analysis of the decomposition of metal carbonyls and relied on a substantial extrapolation of kinetic parameters. The temperature of sonoluminescence determined directly from our C_2 emission spectra is within the error limits of the previous sonochemical results. There are, however, significant experimental differences between the conditions used in the two studies. The vapor pressure in the sonoluminescence determination [~0.01 torr (*23*)] is much lower than in the comparative rate thermometry study (5.0 torr). This might have been expected to increase the temperature of the cavitation event, because of an increase in the polytropic ratio ($\gamma = C_p/C_v$), and a decrease in the isothermal condensation of vapor during collapse (*1, 24*). There may also be a compensatory effect from the Ar sparging used for the sonoluminescence spectra, but not for the comparative rate studies. Sonoluminescence spectra from more volatile hydrocarbons and in the absence of sparging did not give sufficient signal for detailed analysis. From the similarity in measured temperatures at 5.0 and 0.01 torr, it appears that there may be an experimental upper limit to the temperature that can be obtained during cavity collapse.

We have used the sonoluminescence emission of excited-state C_2 as a direct spectroscopic probe of the temperature reached during cavitation. The effective temperature of hot spots created during ultrasonic irradiation of silicone oil is 5075 ± 156 K. The excellent match between the observed sonoluminescence and our synthetic spectra provides definitive proof that the sonoluminescent event is a thermal process and *not* electrical discharge.

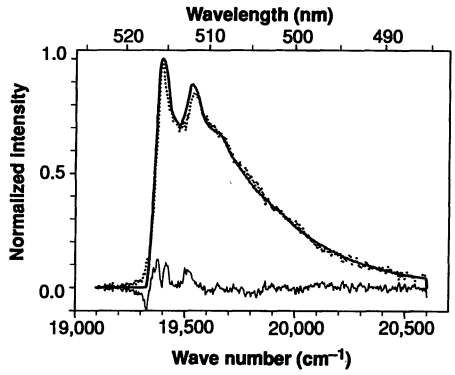

Fig. 2. Emission from the $\Delta v = 0$ manifold of the $d^3\Pi_g - a^3\Pi_u$ transition (Swan band) of C_2. Dotted line shows observed sonoluminescence from silicone oil, as in Fig. 1. Boldface line shows the best-fit synthetic spectrum, with $T_v = T_r$ = 5125 K. Thin line shows the difference spectrum.

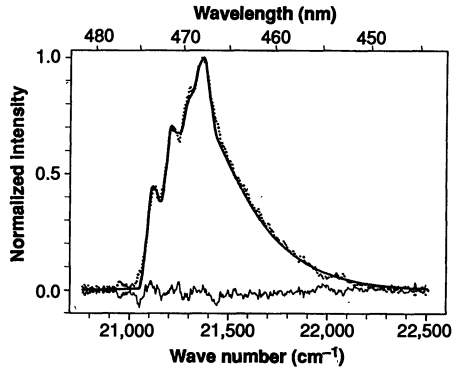

Fig. 1. Emission from the $\Delta v = +1$ manifold of the $d^3\Pi_g - a^3\Pi_u$ transition (Swan band) of C_2. Dotted line shows observed sonoluminescence from silicone oil (polydimethylsiloxane, Dow 200 series, 50 centistokes viscosity) under a continuous Ar sparge at 0°C, vapor pressure ~0.01 torr. Boldface line shows the best-fit synthetic spectrum, with $T_v = T_r$ = 4900 K. Thin line shows the difference spectrum. Sonoluminescence spectra were collected with equipment described in detail elsewhere (*12*). Light emitted during ultrasonic irradiation (Heat Systems Ultrasonics 375 W sonicator equipped with a half-inch horn operating at ~100 W/cm^2) was collimated by a lens onto the slit of a 0.25-m Thermo-Jarrell Ash MonoSpec-18 spectrograph equipped with a 50-μm entrance slit and an 1800-groove-per-millimeter grating; the resolution of the spectrometer was 5.3 cm^{-1}. Dispersed light was detected with a Princeton Instruments IRY 512N diode array detector. Each spectrum is the average of four 100-s spectra and is corrected for variable detector response as a function of wavelength and for light absorption of the solution. An underlying continuum, assigned to C_2H emission (*12*), has been subtracted from each corrected spectrum.

REFERENCES AND NOTES

1. K. S. Suslick, *Science* **247**, 1439 (1990); _____, S. J. Doktycz, E. B. Flint, *Ultrasonics* **28**, 280 (1990). K. S. Suslick, *Sci. Am.* **260**, 80 (February 1989); K. S. Suslick, Ed., *Ultrasound: Its Chemical, Physical, and Biological Effects* (VCH, New York, 1988).
2. C. Einhorn *et al.*, *Synthesis* **11**, 787 (1989); J. Lindley *et al.*, *Chem. Soc. Rev.* **16**, 239 and 275 (1987); K. S. Suslick, *Mod. Synth. Meth.* **4**, 1 (1986).
3. A. J. Walton and G. T. Reynolds, *Adv. Phys.* **33**, 595 (1984); R. E. Verrall and C. Sehgal, in *Ultrasound: Its Chemical, Physical, and Biological Effects*, K. S. Suslick, Ed. (VCH, New York, 1988), pp. 227–287.
4. P. Riesz *et al.*, *Environ. Health Perspect.* **64**, 233 (1985); A. Henglein, *Ultrasonics* **25**, 6 (1987).
5. M. A. Margulis, *Ultrasonics* **23**, 157 (1985); *Adv. Sonochem.* **1**, 39 (1990).

6. R. E. Apfel, in *Ultrasonics: Methods in Experimental Physics*, P. D. Edmonds, Ed. (Academic Press, New York, 1981), vol. 19, pp. 356–413; E. A. Neppiras, *Phys. Rep.* **61**, 159 (1980).
7. M. A. Margulis and A. F. Dmitrieva, *Zh. Fiz. Khim.* **56**, 323 (1982); R. I. Nigmatulin *et al.*, *Int. J. Heat Mass Transfer* **24**, 1033 (1981).
8. D. F. Gaitan and L. A. Crum, in *Frontiers of Nonlinear Acoustics: 12th International Symposium on Nonlinear Acoustics*, M. Hamilton and D. Blackstock, Eds. (Elsevier, New York, 1990), pp. 459–463; A. Prosperetti *et al.*, *J. Acoust. Soc. Am.* **83**, 502 (1988); A. Prosperetti and A. Lezzi, *J. Fluid Mech.* **168**, 457 (1986); L. A. Crum and G. T. Reynolds, *J. Acoust. Soc. Am.* **78**, 137 (1985).
9. S. Fujikawa and T. Akamatsu, *J. Fluid Mech.* **97**, 481 (1980); Y. Matsumoto and F. Takemura, in *Cavitation and Multiphase Flow Forum*, O. Furuya, Ed. (ASME, New York, 1990), pp. 29–34.
10. Lord Rayleigh, *Philos. Mag.* **1917**, 34 and 94 (1917).
11. K. S. Suslick *et al.*, *J. Am. Chem. Soc.* **108**, 5641 (1986); K. S. Suslick *et al.*, *IEEE Trans. Ultrason. Ferroelectr. Freq. Control* **33**, 143 (1986); K. S. Suslick *et al.*, *IEEE Ultrason. Symp.* **1985**, 1116 (1985).
12. K. S. Suslick and E. B. Flint, *Nature* **330**, 553 (1987); E. B. Flint and K. S. Suslick, *J. Am. Chem. Soc.* **111**, 6987 (1989).
13. G. Marr, *Plasma Spectroscopy* (Elsevier, Amsterdam, 1968).
14. G. Herzberg, *Molecular Spectra and Molecular Spectra: Spectra of Diatomic Molecules* (Van Nostrand, New York, 1950) vol. I; K. P. Huber and G. Herzberg, *Molecular Spectra and Molecular Spectra: Constants of Diatomic Molecules* (Van Nostrand, New York, 1979), vol. IV.
15. A. Schadee, *Bull. Astron. Inst. Neth.* **17**, 311 (1964).
16. Attempts were made to record sonoluminescence spectra with a 2-m spectrograph equipped with a 1200-groove-per-millimeter grating and a charge-coupled device detector; the ratio of signal to noise was insufficient to provide usable spectra.
17. M. M. Smit-Miessen and J. L. Spier, *Physica (Amsterdam)* 9, 193 (1942); *ibid.*, p. 442; J. L. Spier and J. A. Smit, *ibid.*, p. 587. In this approach, spectral substructure from J-value splittings and variations in electronic transition moment with v'' are neglected.
18. J. C. McCallum *et al.*, *Spectroscopic Report No. 1* (York University Centre for Research in Experimental Space Science, York, U.K., 1970).
19. G. Stark and S. P. Davis, *Z. Phys. A* **321**, 75 (1985).
20. Attempts to model the CN violet ($B^2\Sigma - X^2\Sigma$) emission from the sonoluminescence of silicone oil under 20% N_2 in Ar were less successful. The experimental spectrum appeared to originate from molecules that were not fully thermally equilibrated. This is not unusual for CN formed from the extremely exothermic reaction of carbon atoms and nitrogen atoms [M. R. Gorbal and M. I. Savadatti, *J. Quant. Spectrosc. Radiat. Transfer* **26**, 457 (1981)].
21. Recent data indicate sonoluminescence lifetimes in water may be as short as 100 ps; given the high pressures during cavitation, thermal equilibration of C_2 is still likely (B. P. Barber and S. Putterman, *Nature* **352**, 318 (1991).
22. E. B. Flint and K. S. Suslick, *J. Phys. Chem.* **95**, 1485 (1991).
23. *Information about Silicone Fluids* and *Vapor Pressure Data of Dow Corning 200 Fluids*, available from C. Kovarik (Dow Corning, Midland, MI).
24. P. Kruus, M. O'Neill, D. Robertson, *Ultrasonics* **28**, 304 (1990); K. S. Suslick, J. W. Gawienowski, P. F. Schubert, H. H. Wang, *ibid.* **22**, 33 (1984); *J. Phys. Chem.* **87**, 2299 (1983).
25. We thank A. Scheeline, J. M. Lisy, and S. W. Rynders for useful discussions on the calculation of synthetic spectra. Supported by the NSF.

29 April 1991; accepted 29 July 1991

The Role of Magma Overpressure in Suppressing Earthquakes and Topography: Worldwide Examples

TOM PARSONS AND GEORGE A. THOMPSON

In an extending terrane basaltic magma supplied at a pressure greater than the least principal stress (overpressure) may be capable of suppressing normal faulting and the earthquakes and topographic relief that commonly accompany normal faulting. As vertical dikes intrude, they press against their walls in the direction opposite the least principal stress and increase its magnitude. The emplacement of tabular intrusions causes the internal magma pressure to act selectively in opposition to tectonic stresses. This process tends to equalize the stresses and thus diminishes the deviatoric stress (difference between maximum and minimum stresses) that creates faults and causes earthquakes. Observations of the pattern of seismicity and magmatism worldwide indicate that magmatism commonly supplants large earthquakes as the primary mechanism for accommodating tectonic extension. Recognizing the extent of magmatic stress accommodation is important in assessing seismic and volcanic risks.

A GENERAL, BUT VARIABLY EXpressed, association between magmatic activity and tectonic extension is recognized worldwide. The association is not uniform. In some rifts, igneous rocks are scarce or absent at the surface, but their presence at depth is suggested by the high heat flow or thermally elevated lithosphere. We suggest that in the seismogenic upper crust, two end-member processes, normal faulting and magmatic intrusion, work together to accommodate extension in varying proportion depending upon magma supply. Below the seismogenic zone, extension is accommodated primarily by ductile flow in the lower crust (*1*). The high speed that dikes propagate relative to the ductile flow rate allows them to penetrate the lower crust, which acts elastically over the short duration of intrusion.

Department of Geophysics, Stanford University, Stanford, CA 94305.

Basaltic magmatism is of particular tectonic importance because it results from partial melting in the Earth's mantle at depths where the density differences between solid and fluid can produce a large buoyant driving pressure. The low viscosity of basaltic relative to more silicic melts (*2*) causes the melts to be intruded as tabular vertical dikes or horizontal sills (*3*). Tabular intrusions are by their geometry able to affect primarily a single component of the stress field, whereas the radially symmetric intrusions produced by more viscous silicic melts tend to have a more uniform effect on the stress field.

In the brittle upper crust tectonic extension in one horizontal direction can be accommodated by normal faulting, in which vertical thinning occurs at constant volume, or by vertical dike injection perpendicular to the extension direction, which increases the rock volume. Complementary extension in one horizontal direction and contraction in another can take place by strike-slip faulting, in which both a constant surface area and constant volume are maintained. Oblique normal faulting represents hybrid behavior between these end members.

We suggest that basaltic magma supplied at a pressure greater than the least principal stress is capable of suppressing normal faulting and the earthquakes and topography that commonly accompany normal faulting. Such magma pressure would also tend to suppress strike-slip faulting.

In normal faulting, the least principal stress is horizontal and in the direction of extension (Fig. 1A). The vertical principal stress, consisting of the lithostatic load, is maximum (*4*). We follow the convention of giving compressional stress in the earth a positive sign. Normal faults fail by shear in response to this maximum principal stress (*5, 6*). Conversely dikes intrude along vertical planes of tension fracturing perpendicular to the least principal stress. In the upper crust (~15 km thick), elastic strain can be stored during slow tectonic extension and episodically released when shear strength is exceeded, a fault slips suddenly, and an earthquake is produced. During this cycle, which generally has a period of hundreds to thousands of years at any given locality, the least principal stress decreases and then suddenly increases at the moment of rupture. The vertical principal stress, governed by the lithostatic load, remains constant. In other words, the deviatoric stress reaches a maximum value and then decreases toward zero during rupture.

Rapid, episodic dike injections cause a similar cycling of stress. When a vertical dike